Dynamical Model of Bubble Path Instability

Woodrow L. Shew and Jean-François Pinton

Laboratoire de Physique de l'École Normale Supérieure de Lyon, CNRS UMR5672, 46 allée d'Italie F-69007 Lyon, France

(Received 18 May 2006; published 6 October 2006)

Millimeter-sized air bubbles rising through still water are known to exhibit zigzag and spiral oscillatory trajectories. We present a system of four ordinary differential equations which effectively model these dynamics. The model is based on Kirchhoff's equations and several physical arguments derived from our experimental observations. In the framework of this model, the zigzag and the spiral motions result from the same underlying bifurcation to wake instability.

DOI: 10.1103/PhysRevLett.97.144508 PACS numbers: 47.55.dd, 47.20.Ky

Oscillatory movement is a common behavior of a body in motion with respect to its fluid environment: a coin settling to the bottom of a fountain, a piece of falling paper, the flutter of an aircraft wing. The body experiences hydrodynamic forces which depend on the body's motion and concurrently change that motion. These nonlinear interactions are responsible for the zigzag and spiral trajectories of small bubbles rising through a still liquid. Such bubble path instabilities have fascinated researchers for centuries, and yet a satisfactory understanding of the underlying physical mechanisms has been elusive.

A number of experimental and numerical studies have revealed the following essential features of the dynamics of a millimeter-sized air bubble rising in water. (We caution the reader that certain experimental conditions such as large diameter bubble generation tubes and surface-active fluid contaminants may dramatically change bubble behavior [1]; hence, the following description as well as our model may not apply in these situations.) The bubble first rises along a straight vertical line and then develops a zigzag motion confined to a vertical plane which subsequently evolves into a spiraling circular motion, at the same frequency as the preceding zigzag [1–8]. Such a bubble trajectory measured in our own experiments [8,9] is shown in Fig. 1. Throughout these dynamics, the bubble maintains an oblate ellipsoidal shape. Observations of the flow in the bubble wake reveal that, the moment the path begins to diverge from vertical, the flow bifurcates from an axisymmetric shape to a pair of long thin vortices reminiscent of the wing-tip vortices produced by an airplane [3–7]. It has been suggested that the wake forms when vorticity production around the bubble exceeds a threshold beyond which the axisymmetric wake no longer evacuates vorticity at a sufficient rate [5,6]. The two wake vortices rotate in opposite directions and align their rotation axes parallel to the path. During the zigzag, the wake vortices break and reform with reversed sense of rotation every time the bubble passes near the inflection point of the zigzag motion [4,6]. During the spiral, the wake is continuously generated. Although it is not universally accepted, many researchers have speculated that the wake vortices effectively pump fluid in a direction normal to the bubble path, which induces a lift force on the bubble in the opposite direction. Our experiments indicate that this lift force plays a crucial role in the oscillatory path instabilities.

Bubble path instabilities occur when the Reynolds number ($\mathrm{Re} = 2RU/\nu$, R equivalent spherical radius, U speed, ν liquid viscosity) of the bubble exceeds a threshold of the order of 10^3. At such values, the system is a very complex two-phase flow. This makes analytical treatment of the full problem unfeasible. Furthermore, a direct numerical approach may be possible, but not without significant computational resources [6,10]. In this Letter, we present a phenomenological model which condenses observations about the wake and forces acting on the bubble into a set of four ordinary differential equations (ODEs) which account for the zigzag and spiral path instabilities. Successful models of free falling plates and strips have used a similar approach (e.g., [11,12]).

The starting point for our model is provided by Kirchhoff's equations. Derived from a Lagrange principle applied to the kinetic energy of the fluid displaced by a submerged body, Kirchhoff's equations specify the angular and linear velocity of the body in terms of the torques and forces, such as drag, lift, and buoyancy, acting upon it (e.g., [10,13]). In the limit of vanishing Reynolds numbers, the

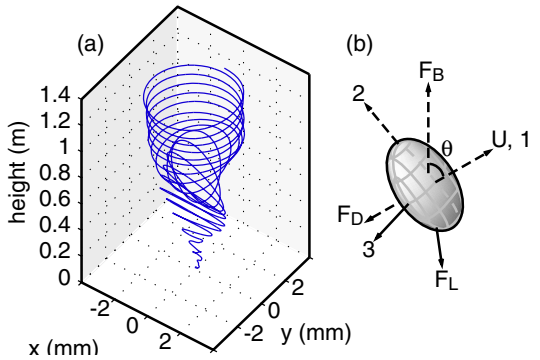

FIG. 1 (color online). (a) An example (from experiments) of a bubble trajectory undergoing zigzag and then spiral motions. (b) Illustration of bubble coordinate system.

hydrodynamical forces acting on the body are explicitly determined (e.g., [14]). As the Reynolds number grows to finite values, these forces must be modified based largely on empirical evidence in order to account for more complex dynamics [15,16]. In the same tradition, our model is based on experimental observations of forces, notably with a wake-dependent lift force.

Kirchhoff's equations for an ellipsoidal bubble are [9]

$$\mathbb{A}_{11}\frac{dU}{dt} = F_1, \qquad \Omega_3\mathbb{A}_{11}U = F_2, \qquad -\Omega_2\mathbb{A}_{11}U = F_3, \tag{1}$$

$$\mathbb{D}_{ii}\frac{d\Omega_i}{dt} = \Gamma_i, \qquad (i = 1, 2, 3), \tag{2}$$

where $(\Omega_1, \Omega_2, \Omega_3)$ is angular velocity. The added mass and added rotational inertia tensors are $\mathbb{A}$ and $\mathbb{D}$, respectively. The components of forces and torques, respectively, on the bubble are F_i and Γ_i. We assume forces consisting of drag F_D, buoyancy F_B, and lift F_L. The 1, 2, and 3 directions define a coordinate system—see Fig. 1(b)—which rotates with the bubble. The 1 direction is defined by the direction of the bubble velocity. The 2 direction is orthogonal to the 1 direction and such that the 1-2 plane is vertical. The positive 2 direction coincides with the 2 component of buoyancy. Finally, the 3 direction is orthogonal to the 1 and 2 directions and, hence, is always horizontal. Quantities are evaluated in the lab frame (Galilean) and projected onto this right-handed, Cartesian, coordinate system. The six equations (1) and (2) are reduced to three using the observational constraint that the short axis of the ellipsoidal bubble remains aligned with the bubble path [6,7], so that

$$\Omega_1 = \frac{d\phi}{dt}\cos\theta, \qquad \Omega_2 = \frac{d\phi}{dt}\sin\theta, \qquad \Omega_3 = -\frac{d\theta}{dt}, \tag{3}$$

where θ is the pitch angle of the path, and ϕ is the azimuthal angle between a fixed horizontal line and the horizontal projection of the 1 direction. Applying this constraint, we are left with

$$\mathbb{A}_{11}\frac{dU}{dt} = F_D + F_{B1}, \tag{4}$$

$$-\frac{d\theta}{dt}\mathbb{A}_{11}U = F_{L2} + F_{B2}, \tag{5}$$

$$-\frac{d\phi}{dt}\sin\theta\mathbb{A}_{11}U = F_{L3}. \tag{6}$$

To proceed further, the buoyancy, drag, and lift forces must be expressed in terms of the dynamic variables U, θ, and ϕ. The components of buoyancy are $F_{B1} = \rho V g\cos\theta$ and $F_{B2} = \rho V g\sin\theta$, where ρ is liquid density, g acceleration due to gravity, and V bubble volume. The drag is taken to be $F_D = -\frac{1}{2}C_D\pi\rho R^2U^2$, where Moore's theory [17] for high Reynolds number bubbles prescribes the drag coefficient $C_D(\chi, \mathrm{Re})$. The bubble aspect ratio (ratio of the long to the short axis) is $\chi(U, R, \rho, \sigma)$, and σ is the surface tension of the air-water interface. As the bubble velocity varies, so does the instantaneous Reynolds number and χ and, hence, the drag force [18]. We note that Moore's theory [17] correctly predicts experimentally measured drag (within 1% for spiral, 8% for zigzag), although it is not strictly valid for the dynamical conditions present in our model and should be viewed only as an effective means of estimating drag. Unlike drag, no theory or quantitative model exists for the lift force. In Fig. 2(a), we present our experimental measurements of the lift force as a function of bubble speed during the entire trajectory shown in Fig. 1(a). The lift force is zero until the zigzag begins at a critical speed of about 36 cm/s. During the zigzag, the lift shows cyclic hysteretic behavior: Nonzero lift persists while the velocity drops below 36 cm/s, finally settling at a constant lift of about 20 μN at a speed less than 35 cm/s for the spiral (see also Fig. 3). We suppose that the lift force is tied to the state of the wake as discussed above and that the wake bifurcation occurs when the vorticity production surpasses a critical value. The vorticity generated at the free-slip boundary of a bubble increases when either the bubble speed or the surface curvature is increased and may be estimated as $\omega \sim U\kappa$, where κ is the surface curvature (e.g., p. 366 in Ref. [20]). For an ellipsoidal bubble, most of the vorticity is generated around its middle where the curvature is greatest $\kappa \sim \chi^{5/3}/R$ (from geometrical considerations). We thus require that the lift force grows when $\omega = U\chi^{5/3}/R$ exceeds a critical value ω_c. While we emphasize that the nature of this bifurcation remains open to debate, we propose that it is subcritical. We are led to this proposition by the hysteresis shown in Fig. 2(a) as well as a second experimental observation [Fig. 2(b)], which reveals an abrupt increase in the amplitude of path oscillations for increasing bubble size. Furthermore, Mougin and

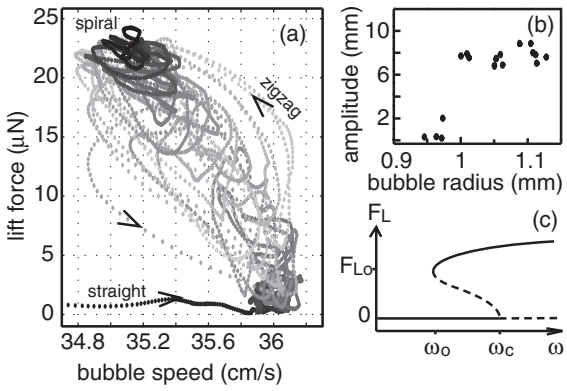

FIG. 2. (a) Evolution of the lift force with bubble speed during an experimental bubble trajectory (gray scale: dark at $t = 0$, light at $t = 2$ s, dark at $t = 4$ s). (b) (Experimental) amplitude of path oscillation increases abruptly for increasing bubble size. (c) Subcritical bifurcation illustration for lift F_L vs vorticity production ω.

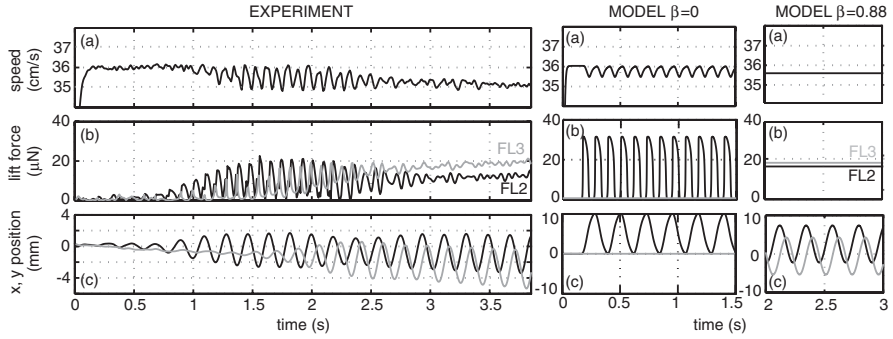

FIG. 3. (a) Bubble speed, (b) lift (F_{L2}, black line; F_{L3}, gray line), and (c) horizontal position for (left) an experimental bubble trajectory, (middle) a model time series during zigzag ($\beta = 0$), and (right) a model time series during spiral ($\beta = 0.88$).

Magnaudet have shown numerical evidence for a subcritical transition to path instability with increasing χ and fixed volume [6]. On the other hand, Mougin and Magnaudet have also shown that, for increasing volume and fixed χ, the transition is supercritical, which may explain the fact that fixed χ bodies (e.g., solid spheres) are observed to have a supercritical transition to the two vortex wake. We thus model the evolution of the lift force with a dynamical equation having the structure of a subcritical bifurcation, namely,

$$\tau \frac{d}{dt}\frac{F_L}{F_{L0}} = k\frac{F_L}{F_{L0}} + k'\left[\left(\frac{F_L}{F_{L0}}\right)^3 - \left(\frac{F_L}{F_{L0}}\right)^5\right], \quad (7)$$

with $k = (\omega - \omega_c)/\omega_c$ and $k' = (\omega_c - \omega_0)/\omega_c$. The lowest stable, nonzero lift force is F_{L0}, and the corresponding ω value is ω_0, as illustrated in Fig. 2(c). Finally, rewriting Eqs. (4)–(6) in terms of the dynamic variables, we obtain the set of ODEs

$$\frac{dU}{dt} = -\frac{3C_D U^2}{8C_M R} + \frac{g\cos\theta}{C_M}, \quad (8)$$

$$\frac{d\theta}{dt} = -\frac{g\sin\theta}{C_M U} + \frac{F_L\cos\beta}{\rho V C_M U}, \quad (9)$$

$$\frac{d\phi}{dt} = \frac{F_L\sin\beta}{\rho V C_M U\sin\theta}, \quad (10)$$

$$\frac{dF_L}{dt} = \frac{1}{\tau}\left(\frac{U\chi^{5/3}/R - \omega_c}{\omega_c}F_L + k'\frac{F_L^3}{F_{L0}^2} - k'\frac{F_L^5}{F_{L0}^4}\right), \quad (11)$$

where $C_M = \mathbb{A}_{11}/\rho V$ is the added mass coefficient for motion parallel to the short axis of the bubble. The angle β specifies the projection of the lift force onto the 2 and 3 directions. Physically, β is related to the orientation of the plane which contains the two wake vortices; it is the angle between this plane and the plane defined by the 1 and 3 directions. During the zigzag, F_{L3} is zero (the motion is planar), so that $\beta = 0$ and $F_{L2} = F_L$. During the spiral, neither lift component is zero and both are steady in time: $F_{L2} = F_L\cos\beta$, $F_{L3} = F_L\sin\beta$, with β constant. In the lift force equation, τ is a characteristic time for growth or decay of the wake. We suppose τ is an advective time scale $\tau = R/U_a$, with U_a given by a balance of drag and buoyancy $U_a \sim R^2 g/\nu$, so that $\tau = \nu/Rg$.

We now compare details of the model behavior to experimental measurements. In our experiments, an ultrasound device and a camera are used to make precise measurements of the bubble trajectories as they rise through 2 m of water. The bubbles are generated with a small diameter tube (0.3 mm) to ensure an ellipsoidal shape (''pinch-off method'' according to Ref. [1]). The details of the method and procedures are presented in Ref. [9]. We first provide a brief summary of our experimental findings as well as some from other studies, restricting attention to ellipsoidal bubbles generated from a small tube in relatively clean water. Zigzag and spiral motions are observed when the bubble volume exceeds 3.82 mm^3 (i.e., $R >$ 0.97 mm) [9,19]. The zigzag is sinusoidal motion confined to a vertical plane, 5–10 mm in amplitude and about 5 Hz in frequency [1,2,4,6,8,9]. The speed of a zigzagging bubble oscillates between its terminal speed (maximum speed at the end of the straight rise), about 36 cm/s, and 1–2 cm/s slower. Bubbles are more commonly observed to spiral than zigzag, and a bubble which first zigzags always spirals eventually. Projected onto a horizontal plane, fully developed spiral motion is circular, 5–10 mm in radius [1–9], and at the same frequency as the preceding zigzag [8,9]. The speed of the spiraling bubble is constant and 1–2 cm/s slower than the terminal speed.

We first consider the model predictions when β is set to zero. In the numerical implementation of the model, the only free parameters are $F_{L0} = 20\ \mu$N, $\omega_0 = 1.13 \times 10^3$ 1/s, and $\omega_c = 1.17 \times 10^3$ 1/s, which are inferred from the experimental measurements—Fig. 2. Figure 3 shows bubble speed, lift forces, and horizontal bubble position for an entire experimental trajectory (left) and the numerical results for $\beta = 0$ (middle). One indeed observes a straight rise followed by a zigzag motion (wake reversals which occur during the zigzag and change the direction of the lift are implemented numerically by changing the sign of F_L once each time it drops below a small threshold value). Compared to the experiment, we find very good agreement for the period of oscillation, the amplitude of motion, and the magnitude of the lift force. Note that it is the response time in the velocity equation $\tau_U \approx 8C_M R/3C_D U \sim 0.1$ s which sets the characteristic

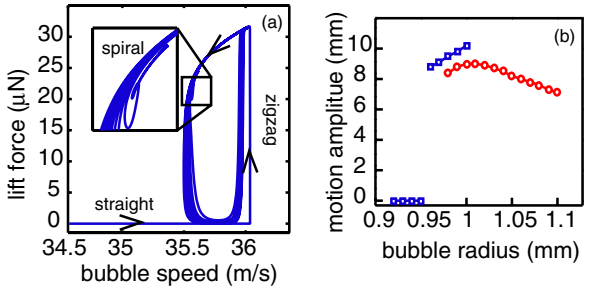

FIG. 4 (color online). (a) Magnitude of lift force as a function of bubble speed during a model trajectory. (b) Amplitude of model path oscillations for a range of bubble sizes (□, zigzag; ○, spiral).

period of oscillation, rather than the advective time $\tau = \nu/Rg \sim 10^{-4}$ s.

In Fig. 3 (right), the model equations are solved with $\beta = 0.88$; all other parameters are unchanged. We find that the motion indeed evolves into a spiral quite similar to that observed in experiments. The value of β was chosen based on our experimental measurements of β during the spiral state, which ranges between 0.85 and 1 for bubbles with the radius between 1 and 1.12 mm. By solving the model equations in the steady spiral state, we uncover a link between β and the spiral frequency. One obtains $\dot{\phi} = g\tan\beta/C_M U_s$, with U_s the steady spiral velocity.

Figure 4(a) shows the total magnitude of the lift force as a function of bubble speed for the model. This result may be compared with the experimental data presented in Fig. 2(a). In both the experiment and the model, it is clear that, in the spiral state, the lift force persists at a lower speed than the speed at which the path became unstable. During the zigzag, the bubble makes loops in the F_L-U plane, finally settling to a point during the spiral. In the context of the model, the underlying physics is the following. As long as the angle β is zero, an increase in lift force necessarily leads to a decrease in velocity. Changes in F_L drive changes in the pitch angle θ, which, in turn, drive changes in the speed U. But, when β becomes nonzero, a fraction of the lift force is diverted into driving changes in ϕ instead of θ. This shift of F_L partially into F_{L3} is what allows the lift force to persist at a lower velocity in the spiral state. Finally, in Fig. 4(b), we present the onset and amplitude oscillatory motions of the model, which compare favorably with our experimental measurements shown in Fig. 2(b). Note that the largest bubble size for which a zigzag (squares) exists as a solution to the model is about 1 mm, and the smallest size with a spiral solution (circles) is about 0.98 mm. Although these limits may be artifacts of the model, they might also point to the reason that experiments typically see zigzag motion followed by spiral motion and never the reverse.

To conclude, we have presented a simple dynamical system of four ordinary differential equations which effectively reproduce the zigzag and spiral motions of millimeter-sized ellipsoidal air bubbles rising in water. We present good qualitative and quantitative agreement with experimental measurements of zigzag and spiral path oscillation amplitude, frequency, as well as dynamics of lift forces. Future improvements may entail a fifth ODE governing β, i.e., the nontrivial dynamics of the relative magnitudes of F_{L2} and F_{L3} (see Fig. 3). Furthermore, a more realistic drag force likely depends on the wake dynamics, analogous to the lift force.

We appreciate Jacques Magnaudet's helpful advice on Kirchhoff's equations. This work was partially funded by the Région Rhône-Alpes, under Emergence Contract No. 0501551301.

[1] M. Wu and M. Gharib, Phys. Fluids **14**, L49 (2002).
[2] N. M. Aybers and A. Tapucu, Wärme- Stoffübertrag. **2**, 118 (1969); **2**, 171 (1969).
[3] C. Brücker, Phys. Fluids **11**, 1781 (1999).
[4] A. W. G. de Vries, A. Biesheuvel, and L. van Wijngaarden, Int. J. Multiphase Flow **28**, 1823 (2002).
[5] K. Lunde and R. J. Perkins, in *Proceedings of the 1997 ASMEFED Summer Meeting, Vancouver, Canada* (American Society of Mechanical Engineers, New York, 1997).
[6] G. Mougin and J. Magnaudet, Phys. Rev. Lett. **88**, 014502 (2002).
[7] K. Ellingsen and F. Risso, J. Fluid Mech. **440**, 235 (2001).
[8] W. L. Shew and J.-F. Pinton, J. Stat. Mech. (2006) P01009.
[9] W. L. Shew, S. Poncet, and J.-F. Pinton (to be published).
[10] G. Mougin and J. Magnaudet, Int. J. Multiphase Flow **28**, 1837 (2002).
[11] P. Pesavento and Z. J. Wang, Phys. Rev. Lett. **93**, 144501 (2004).
[12] A. Belmonte, H. Eisenberg, and E. Moses, Phys. Rev. Lett. **81**, 345 (1998).
[13] M. S. Howe, Q. J. Mech. Appl. Math. **48**, 401 (1995).
[14] M. R. Maxey and J. J. Riley, Phys. Fluids **26**, 883 (1983).
[15] J. Magnaudet and I. Eames, Annu. Rev. Fluid Mech. **32**, 659 (2000).
[16] R. Clift, J. R. Grace, and M. E. Weber, *Bubbles, Drops, and Particles* (Academic, New York, 1978).
[17] D. W. Moore, J. Fluid Mech. **23**, 749 (1965).
[18] Strictly applied, Kirchhoff's equations are valid for rigid bodies, but we loosen this restriction and allow for small changes (5%) in χ using Moore's theory with a constant correcting factor in order to agree with experiments [19].
[19] P. C. Duineveld, J. Fluid Mech. **292**, 325 (1995).
[20] G. K. Batchelor, *An Introduction to Fluid Dynamics* (Cambridge University Press, Cambridge, England, 1967).